energies

MDPI

Article

Applicability of Wake Models to Predictions of Turbine-Induced Velocity Deficit and Wind Farm Power Generation

Dongqin Zhang [1], Yang Liang [1], Chao Li [1], Yiqing Xiao [1] and Gang Hu [1,2,3,*]

[1] School of Civil and Environmental Engineering, Harbin Institute of Technology, Shenzhen 518055, China
[2] Shenzhen Key Laboratory of Intelligent Structure System in Civil Engineering, Harbin Institute of Technology, Shenzhen 518055, China
[3] Guangdong-Hong Kong-Macao Joint Laboratory for Data-Driven Fluid Mechanics and Engineering Applications, Harbin Institute of Technology, Shenzhen 518055, China
* Correspondence: hugang@hit.edu.cn

Abstract: Turbine-induced velocity deficit is the main reason to reduce wind farm power generation and increase the fatigue loadings. It is meaningful to investigate turbine-induced wake structures by a simple and accurate method. In this study, a series of single turbine wake models are proposed by combining different spanwise distributions and wake boundary expansion models. It is found that several combined wake models with high hit rates are more accurate and universal. Subsequently, the wake models for multiple wind turbines are also investigated by considering the combined wake models for single turbine and proper superposition approaches. Several excellent plans are provided where the velocity, turbulence intensity, and wind power generation for multiple wind turbines can be accurately evaluated. Finally, effects of thrust coefficient and ambient turbulence intensity are studied. In summary, the combined wake models for both single and multiple wind turbines are proposed and validated, enhancing the precision of wind farm layout optimization will be helped by using these wake models.

Keywords: theoretical wake model; wake boundary expansion; added turbulence intensity; superposition approach; wind power generation

Citation: Zhang, D.; Liang, Y.; Li, C.; Xiao, Y.; Hu, G. Applicability of Wake Models to Predictions of Turbine-Induced Velocity Deficit and Wind Farm Power Generation. *Energies* **2022**, *15*, 7431. https://doi.org/10.3390/en15197431

Academic Editors: Esmaeel Eftekharian, Robert H. Ong and João Carlos de Campos Henriques

Received: 30 July 2022
Accepted: 4 October 2022
Published: 10 October 2022

1. Introduction

Wind energy is considered as one of most clean renewable resources and the exploitation of wind power can help us to solve the energy and environment crises. In 2021, the wind turbine capacity added 93.6 GW all over the world, and the global cumulative capacity reached 837 GW. However, it has been pointed out by GWEC that four times as much will be needed annually by 2030 to achieve net-zero emission [1]. Therefore, it is necessary to increase the global wind energy investigation and improve the wind power exploitation efficiency.

Theoretical or empirical wake models are widely used to carry out the wind farm layout optimization (WFLO) due to their simplicity and effectiveness. Therefore, an accurate wake model is the premise of the wind farm layout optimization. Jensen [2] firstly proposed an analytical wake model using the top-hat distribution and mass conservation, and this is widely used to conduct the WFLO. Frandsen et al. [3] also proposed an analytical wake model considering both mass and momentum conservation. Subsequently, Gaussian-based wake models were proposed [4,5] to overcome the discrepancy between top-hat distribution and the measured velocity deficit. Cosine-shaped wake models have also been proposed by Tian et al. [6] and Zhang et al. [7]. It is believed that the Gaussian-based or cosine-shaped wake models are more advanced, and they are consistent with the boundary layer theory. In addition, the 3D wake models [8,9], the full wake models [10,11], and the wake model

for offshore wind turbine [12], have also been proposed. All these wake models have been validated by specific experiments or simulations, and wake model comparisons have also been carried out. However, a comprehensive comparison of these wake models with field tests, wind tunnel tests, and numerical simulations has not been carried out and the applicability of these wake models has not been discussed.

There are three main parts of the analytical wake model: the spanwise function, the streamwise function, and the wake boundary expansion model. In general, it is assumed that the spanwise function is distributed as the top-hat, Gaussian, or cosine shape, and the streamwise function can be derived by the spanwise function, the mass and momentum conservation. As for the wake boundary expansion, these are predicted by the empirical models and validated by measured data. The linear wake boundary expansion model with a constant expansion rate is the simplest one [2]. A non-linear model to describe the wake boundary expansion is adopted by Frandsen et al. [3]. To consider the effects of thrust coefficient and ambient turbulence intensity, it is assumed that the expansion rate and the intercept are related to these two parameters by Ishihara and Qian [5]. Furthermore, a non-linear wake boundary expansion model in which the wake radius is influenced with the added turbulence intensity is used [6,7,13]. Researchers have proposed the spanwise distribution, the streamwise function, and the wake boundary expansion model simultaneously, as shown in Table 1, however, the combined wake models (by considering different spanwise distributions, streamwise functions, and wake boundary expansion models) have not been systematically studied.

To calculate the velocity distribution and power generation in the wind farm, the wake velocity needs to be added together properly. A series of empirical superposition approaches for multiple wind turbines have been proposed, including the ambient-based linear superposition approach [14], the rotor-based linear superposition approach [15], the ambient-based root sum square superposition approach [16], the rotor-based root sum square superposition approach [17], the geometric superposition approach [18], and the energy conservation superposition approach [19]. Qian and Ishihara [20] compared the first four superposition approaches and found that the rotor-based linear superposition approach is more suitable for the IQ wake model. Yang et al. [13] and Tian et al. [21] noted that prediction results obtained by the root sum square superposition approach show excellent agreement with numerical simulations. Kirchner-Bossi and Porté-Agel [22] found that the combination of the rotor-based linear superposition approach and the BP wake model is an effective and accurate way to evaluate the wind power generation. The accurate prediction of wind velocity and wind power generation for multiple wind turbines depends on both the single wind turbine wake model and the superposition approach. Therefore, it is necessary to find the suitable superposition approach for a specific single wind turbine wake model.

In this study, the applicability of wake models to predict of turbine-induced velocity deficit and power generation is investigated. Theoretical wake models for single and multiple wind turbines including spanwise and streamwise distributions for velocity deficit, wake boundary expansion, added turbulence intensity, superposition approaches, and the Horn Rev 1 wind farm are introduced in Sections 2 and 3, respectively. The combined wake models for both single and multiple wind turbines are proposed and validations are also carried out, and effects of thrust coefficient and ambient turbulence intensity on the wind power generation are studied in Section 4. Section 5 summarizes the conclusions.

Table 1. Analytical and empirical wake models in the far wake region.

Model	Expression	Wake Boundary Expansion	Application
Jensen [2]	$\frac{\Delta U}{U_0} = \left(1 - \sqrt{1 - C_T}\right)\left(\frac{D}{D_w}\right)^2$	Linear	WFLO [23]
Frandsen et al. [3]	$\frac{\Delta U}{U_0} = \frac{1}{2}\left(1 - \sqrt{1 - 2\frac{A}{A_w}C_T}\right)$	Non-linear	N/A
Bastankhah and Porté-Agel [4]	$\frac{\Delta U}{U_0} = \left(1 - \sqrt{1 - \frac{C_T}{8\left(\frac{\sigma}{D}\right)^2}}\right) exp\left(-\frac{r^2}{2\sigma^2}\right)$	Linear	WFLO [22]
Ishihara and Qian [5]	$\frac{\Delta U}{U_0} = \frac{C_T}{\left[a_1 + b\frac{x}{D} + \frac{c}{\left(1 + \frac{x}{D}\right)^2}\right]^2} exp\left(-\frac{r^2}{2\sigma^2}\right)$	Linear	Wind farm power generation [20]
Zhang et al. [7]	$\frac{\Delta U}{U_0} = \left[\frac{\pi^2 - 4}{3\pi^2 - 16} - \sqrt{\left(\frac{\pi^2 - 4}{3\pi^2 - 16}\right)^2 - \frac{\pi^2 C_T}{3\pi^2 - 16}\left(\frac{r_0}{r_w}\right)^2}\right] \times \left[cos\left(\frac{r}{r_w}\pi\right) + 1\right]$	Non-linear	N/A

2. Wake Models for the Single Wind Turbine

A series of analytical and empirical wake models for prediction of the velocity deficit, wake boundary expansion, and added turbulence intensity are introduced in Sections 2.1–2.3.

2.1. Spanwise and Streamwise Distributions

The mass and momentum conservations of a control volume around a wind turbine can be expressed as:

$$\int_{A_0} \rho U_0 dA = \int_{A_W} \rho U_W dA \tag{1}$$

$$\int_{A_0} \rho U_0^2 dA - \int_{A_W} \rho U_W^2 dA = \frac{1}{2}\rho C_T A_0 U_0^2 \tag{2}$$

where U_0, A_0 represent the inflow wind speed at hub height and the rotor area. U_W, A_W refer to the wind velocity and the cross-sectional area influenced by wake in the downstream distance. ρ shows the density of air and C_T presents the thrust coefficient.

Multiplying U_0 on both side of Equation (1) and then substituting it into Equation (2).

$$\int_{A_W} \rho U_W (U_0 - U_W) dA = \frac{1}{2}\rho C_T A_0 U_0^2 \tag{3}$$

The velocity deficit can be separated into two independent terms including the spanwise term and the streamwise term and expressed as:

$$\frac{\Delta U}{U_0} = 1 - \frac{U_W}{U_0} = C(x)G(r) \tag{4}$$

where $C(x)$ and $G(r)$ are streamwise and spanwise functions of velocity deficit.

The top-hat, Gaussian, and cosine-shaped distributions are three main functions to describe the spanwise velocity as shown in Figure 1. The x axis shows the radial distance

normalized by the wake's half width $r_{1/2}$ and the y axis illustrates the velocity deficit normalized by the inflow wind velocity U_0. The wake's half width $r_{1/2}$ of wake radius is defined as the radial distance where half of the maximum velocity deficit is obtained for Gaussian and cosine-shaped distributions and the half width of wake radius for the top-hat distribution. The Gaussian and cosine-shaped distributions are written in Equations (5) and (6). In accordance with mass and momentum conservation, the streamwise functions can be derived as shown in Table 1. It is distinct that the velocity deficit predicted by the Gaussian or cosine-shaped distribution has one peak, while it maintains a constant value for the whole wake region at a specific downstream distance by the top-hat distribution. Compared with the top-hat distribution, it seems that the Gaussian or cosine distribution is more advanced and realistic since the wake velocity satisfies the boundary layer theory. Furthermore, it is found that the Gaussian distribution reduces to zero more smoothly than the cosine-shaped distribution in Figure 1. In summary, these two distributions are similar and more realistic to depict wake structures than the top-hat distribution.

$$G(r) = exp\left(-\frac{r^2}{2\sigma^2}\right) \tag{5}$$

$$G(r) = \frac{1}{2}\left[cos\left(\frac{\pi}{r_w}r\right) + 1\right] \tag{6}$$

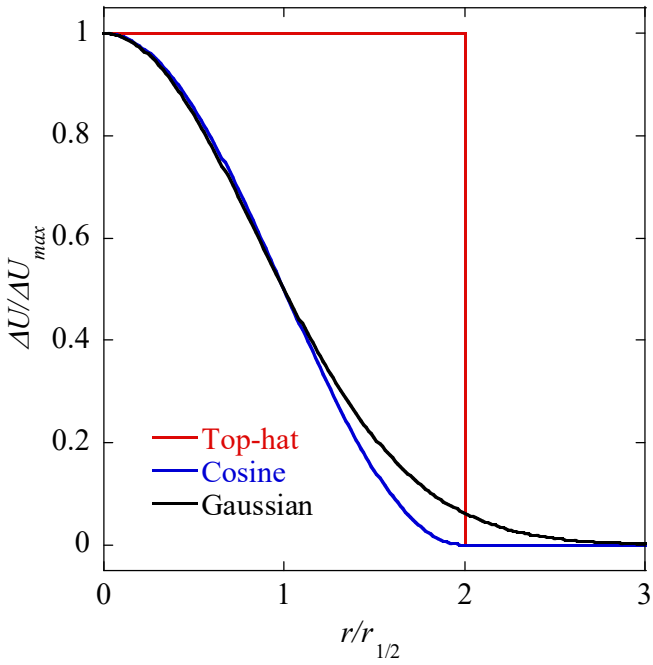

Figure 1. Spanwise distribution of velocity deficit.

The applications of these three spanwise distributions are summarized in Table 1. Theoretical wake models with a top-hat distribution are widely used to carry out WFLO due to their simplicity. In recent years, the Gaussian-based and cosine-shaped wake models have been proposed and the prediction results match well with experimental data. In accordance with mass and momentum conservation and the assumption of spanwise distribution, the streamwise function can be easily derived, such as the top-hat model [3], the Gaussian model [4,5], and the cosine-shaped model [7]. The wake model [5] is considered as a new Gaussian-based wake model since the streamwise function derived by Bastankhah and Porté-Agel [4] is decomposed by Taylor expansion and the only first order is kept.

2.2. Wake Boundary Expansion

The wake expands with the streamwise distance due to the flow mixing at the wake boundary. In general, the empirical formulas of the wake boundary expansion are proposed by using numerical or experimental results since it cannot be directly derived from the mass and momentum conservations.

The linear formula with a constant expansion rate to present the wake expansion is the simplest model. The wake expansion rate is defined as 0.075 [24] for the onshore wind farm while it is equal to 0.04 [25,26] or 0.05 [24,27] for the offshore wind farm. In fact, both thrust coefficient and ambient turbulence intensity have significant effects on the wake expansion rate. For example, the higher ambient turbulence intensity will accelerate the flow mixing and will induce a larger wake expansion rate. To meet this principle, the complicated expressions to describe the wake expansion are proposed, including the linear expression model where the wake expansion rate is related to thrust coefficient and ambient turbulence intensity, and the non-linear formula where the wake expansion is determined by the aerodynamic surface roughness, ambient, and added turbulence intensities. Table 2 summarizes empirical models proposed by previous studies to describe the wake boundary expansion.

Furthermore, to illustrate the relationship between the wake radius r_w and the standard deviation of velocity deficit σ, the following two expressions are widely used [5,28].

$$\sigma = \frac{r_w}{2} \tag{7}$$

$$\sigma = \frac{r_w}{2\sqrt{2ln2}} \tag{8}$$

Table 2. Empirical models for wake boundary expansion.

Ref	Principle	Expression	Parameters
Jensen [2]	Linear	$\frac{D_W}{D} = k\frac{x}{D} + 1$	$k = 0.05$
Frandsen et al. [3]	Non-linear	$\frac{D_W}{D} = \left(\beta\frac{K}{2} + \alpha\frac{x}{D}\right)^{\frac{1}{K}}$	$\alpha = 0.7$ $K = 3$ $\beta = \frac{1+\sqrt{1-C_T}}{2\sqrt{1-C_T}}$
Ishihara and Qian [5]	Linear	$\frac{\sigma}{D} = k\frac{x}{D} + \varepsilon$	$k = 0.11C_T^{1.07}I_0^{0.2}$ $\varepsilon = 0.23C_T^{-0.25}I_0^{0.17}$
Zhang et al. [7]	Non-linear	$\frac{r_W}{D} = k\frac{x}{D} + 0.5$	$k = k_t\frac{I_W}{I_0}$ $k_t = \frac{0.5}{ln(z_h/z_0)}$

Numerical simulations [29] were carried out to study the effects of ambient turbulence intensity on turbine wake structures and the wake boundary expansions along the downstream distances were calculated. Four cases with different ambient turbulence intensities of 0.134, 0.094, 0.069, and 0.048 were studied. The wake boundary expansions predicted by different models are compared with the numerical simulations [29] in Figure 2. The wake boundary predictions by the Jensen model and the Frandsen model are not influenced by the ambient turbulence intensity, and they maintain the same trend for four cases. It seems that they are parallel with each other when the thrust coefficient is equal to 0.8, although the wake boundary curve predicted by the Frandsen model is non-linear. In addition, the curves predicted that the IQ model shows acceptable agreement with numeri-

cal simulations for all the cases, while the results by the Zhang model are always slightly larger than numerical simulations. The Frandsen model provides an acceptable result only if the ambient turbulence intensity is low, while the Jensen model shows the worst result. Therefore, the linear and non-linear wake boundary expansion models proposed by Ishihara and Qian [5], Zhang et al. [7], and Frandsen et al. [3] are considered in the following contents due to their advantages.

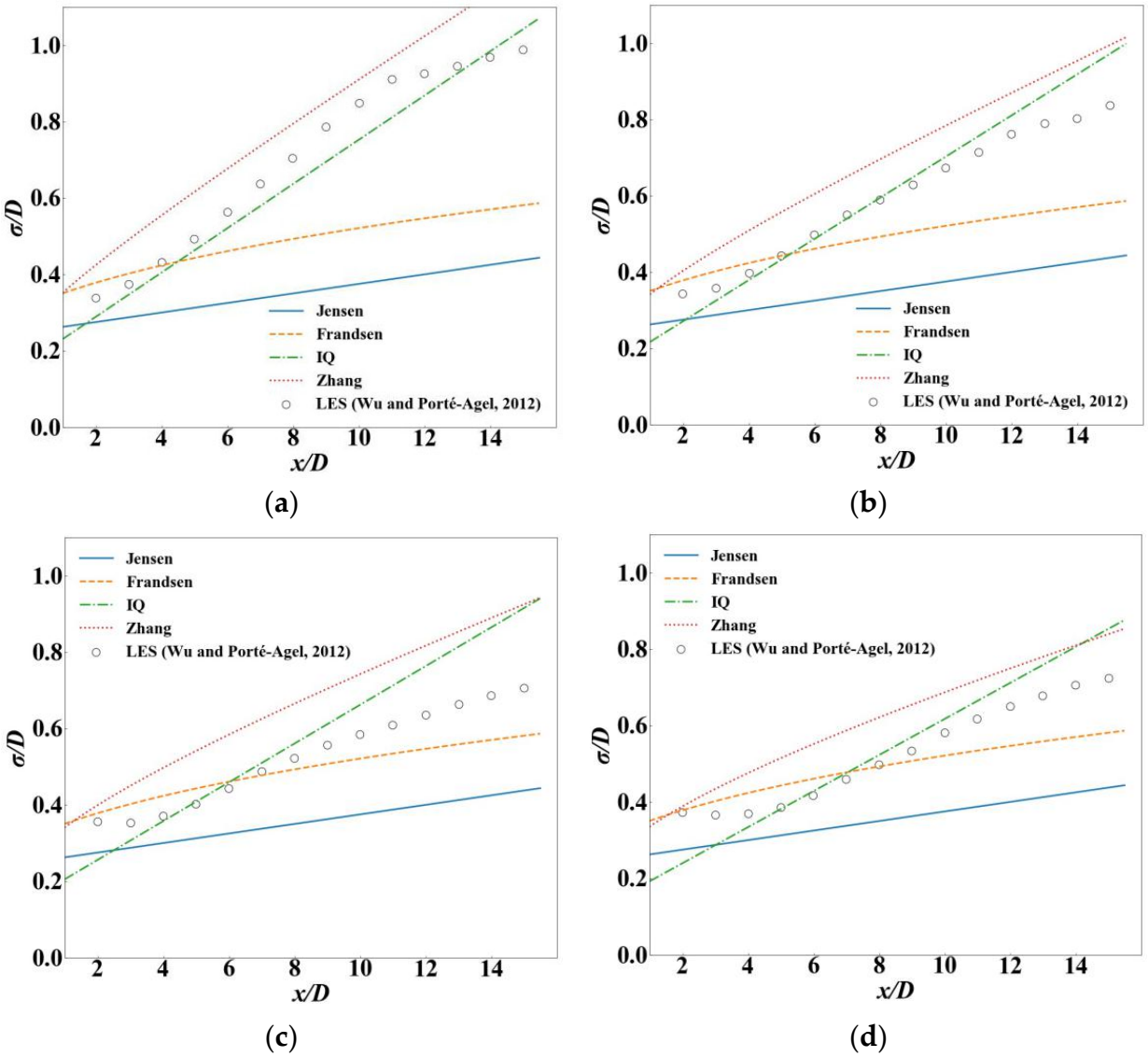

Figure 2. Comparisons of the wake boundary expansion between numerical simulations ($C_T = 0.8$, $z_h = 70\ m$) [4] and the empirical models: (**a**) $I_0 = 0.134$, $z_0 = 0.5\ m$; (**b**) $I_0 = 0.094$, $z_0 = 0.05\ m$; (**c**) $I_0 = 0.069, z_0 = 0.005\ m$; (**d**) $I_0 = 0.048$, $z_0 = 0.00005\ m$.

2.3. Added Turbulence Intensity

The added turbulence intensity will be generated by the rotating blades of the upcoming turbine and they will affect the wake boundary expansion. The higher added turbulence intensity will accelerate the flow mixing with surrounding air. Table 3 summarizes four empirical wake models to describe the streamwise added turbulence intensity. The more advanced wake models to evaluate the added turbulence intensity considering the spanwise distribution are not considered in this study.

Table 3. Wake models for added turbulence intensity.

Ref	Expression	Parameters
Crespo and Hernandez [30]	$I_+ = 0.73a^{0.8325} I_0^{0.0325} (x/D)^{-0.32}$	$a = \frac{1-\sqrt{1-C_T}}{2}$
Frandsen et al. [3]	$I_+ = \sqrt{K_n C_T}/(x/D)$	$K_n = 0.4$
Larsen et al. [31]	$I_+ = 0.29(x/D)^{-1/3}\sqrt{1-\sqrt{1-C_T}}$	N/A
IEC 61400-1 [32]	$I_+ = \frac{1}{1.5+0.8(x/D)/\sqrt{C_T}}$	N/A

Figure 3 illustrates comparison of the streamwise distribution of added turbulence intensity between numerical simulations [5] and empirical models. It is noted that the results by the Crespo and Hernandez model, by the Larsen model, and by IEC model show good agreement with simulations in Figure 3b, in Figure 3c, and Figure 3d, respectively. Compared with other empirical models, the Larsen mode presents acceptable results for all cases. Furthermore, the streamwise added turbulence intensities predicted by the Crespo and Hernandez model and the Larsen model change more smoothly with the downstream distance and they are close to each other. The other two curves by the Frandsen model and the IEC 61400-1 model have the same trends, while the streamwise added turbulence intensity predicted by the IEC 61400-1 model has a higher value. Predictions of the streamwise added turbulence intensity converge in the far wake region, except in the Frandsen model.

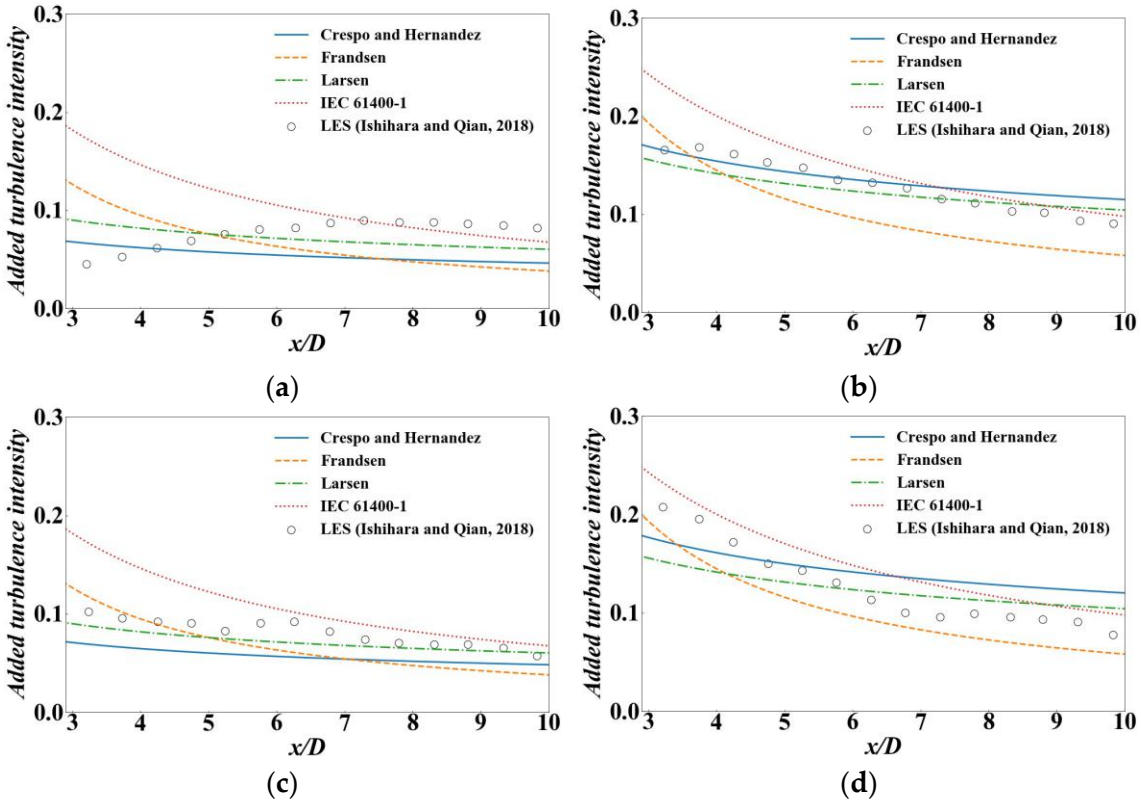

Figure 3. Comparison of the streamwise distributions of added turbulence intensity between numerical simulations [5] and empirical models: (**a**) $I_0 = 0.035$, $C_T = 0.36$; (**b**) $I_0 = 0.035$, $C_T = 0.84$; (**c**) $I_0 = 0.137$, $C_T = 0.36$; (**d**) $I_0 = 0.137$, $C_T = 0.84$.

The turbulence intensity in the wake region can be separated into two parts: the ambient turbulence intensity and the added turbulence intensity. Three superposition approaches are used in the previous studies to generate the turbulence intensity in Table 4. The added turbulence intensity should be modified slightly based on different superposition approaches and the detailed explanations can be found in the references [23,33].

Table 4. Summation of superposition approaches for added turbulence intensity.

Ref	Principle	Expression
Frandsen et al. [3]	Square and root	$I_W = \sqrt{I_0^2 + I_+^2}$
Tian et al. [21]	Linear	$I_W = I_+ + I_0$
Gao et al. [33]	Root and square	$I_W = \left(I_+^{0.5} + I_0^{0.5}\right)^2$

2.4. Summary of the Wake Models

Wake models for the single wind turbine are summarized in this section. As shown in Figure 4, an example of the combined wake model is introduced. The spanwise and streamwise functions are chosen in Table 1. At this moment, it is necessary to calculate wake boundary expansion which cannot derived by the mass and momentum equations. Either the linear or the non-linear empirical models in Table 2 can be used. The added turbulence intensity and the superposition methods for turbulence intensity are selected in Table 3 and in Table 4, respectively, if the non-linear empirical model is adopted. The wake model has been finished if the linear empirical model is chosen. Finally, the combined wake model is proposed. In this study, 70 combined wake models are totally proposed and summarized, including wake models proposed by other researchers, such as the BP model, IQ model, Zhang model, Yang model etc., in Table A1.

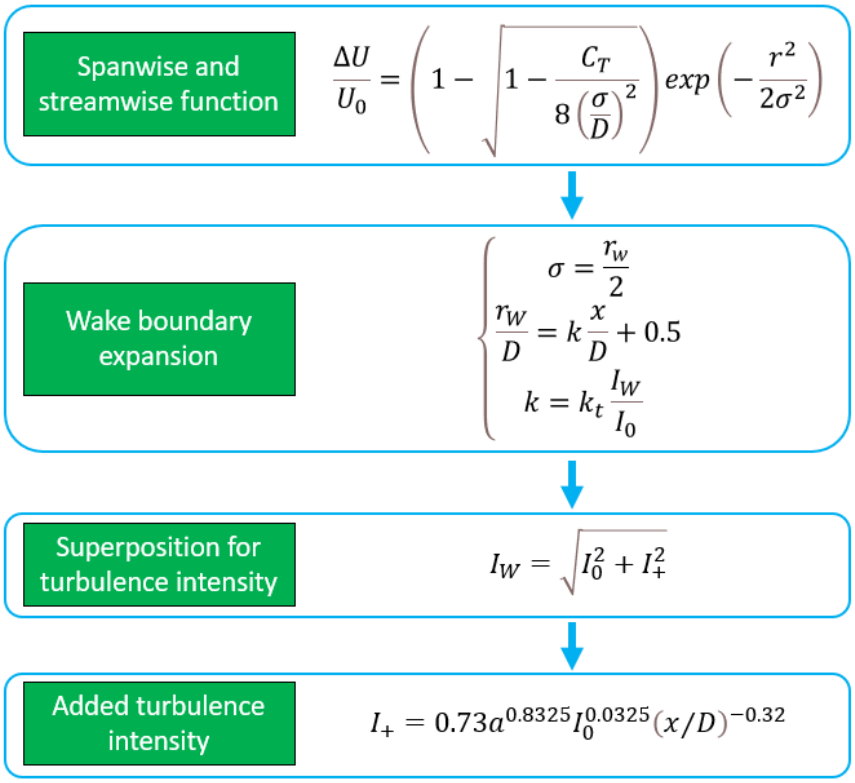

Figure 4. An example of the combined wake model.

3. Wake Models for Multiple Wind Turbines

The superposition approaches to add the wake velocity deficit for multiple wind turbines are presented in Section 3.1 and the Horn Rev 1 offshore wind farm is illustrated in Section 3.2.

3.1. Superposition Approaches

Six superposition approaches are commonly used to add the wake velocity deficit in Table 5. For the ambient-based velocity deficit superposition approach, it is assumed that the space between two wind turbines is large and their interaction between each other can be negligible, so that the inflow velocity of the downstream wind turbine and the whole wind farm are close to each other, i.e., $u_{h,i} \approx u_0$. For the rotor-based velocity deficit superposition approach, the velocity deficit over the whole rotor area of the downstream turbine is not uniform, so the averaged inflow velocity over the whole rotor area is calculated by Equation (9). The velocity deficit can be added together by the linear sum method or the root sum square method. For the energy deficit linear sum method, the square of velocity is considered as a scalar and be summed linearly. It should be pointed out that these six superposition approaches are empirical methods without a rigorous theoretical foundation. It is expected that the rotor-based velocity deficit superposition approach is more accurate, especially for the cases with short turbine spacing, since it avoids the error accumulation of inflow wind velocity from upstream to downstream [15,16].

Wake superposition effects of two wind turbines are shown in Figure 5. It is assumed that the wake velocity deficit generated by the upstream wind turbine (red line) will be superposed to the downstream wake velocity deficit (blue line) and the final velocity deficit is illustrated as the black line.

$$U_{h,i} = \int_{A_0} U dA \tag{9}$$

where U shows the wake velocity at the ith wind turbine in a wind farm.

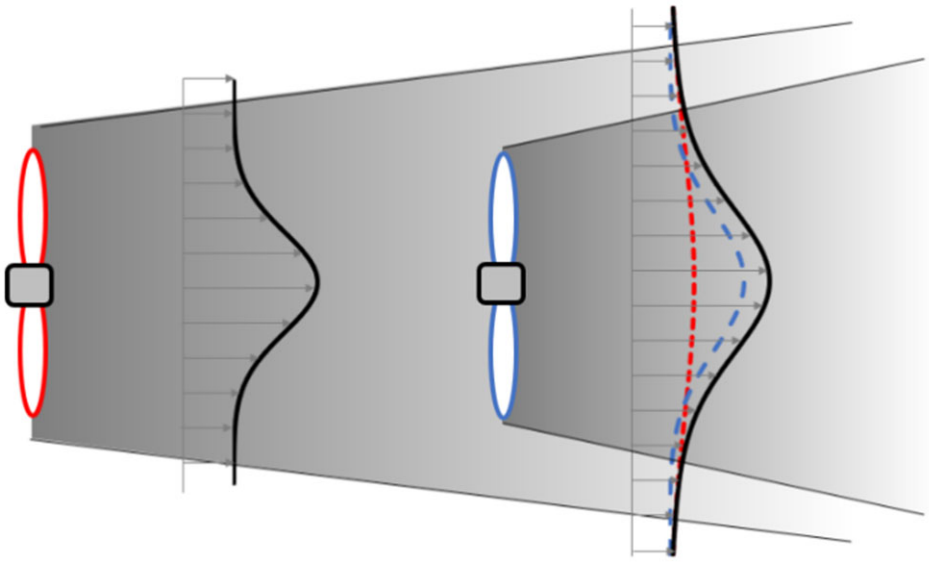

Figure 5. Wake superposition effect of two wind turbines.

Table 5. Superposition approaches of multiple wind turbines.

Wake Superposition Principle	Multiple Wake	Single Wake
Ambient-based velocity deficit linear sum (AVDLS) [14]	$U = U_0 - \sum_{i=1}^{n}(U_0 - U_i)$	$\Delta U_i = U_0 - U_i$
Rotor-based velocity deficit linear sum (RVDLS) [15]	$U = U_0 - \sum_{i=1}^{n}(U_{h,i} - U_i)$	$\Delta U_i = U_{h,i} - U_i$
Ambient-based velocity deficit root sum square (AVDRSS) [16]	$U = U_0 - \sqrt{\sum_{i=1}^{n}(U_0 - U_i)^2}$	$\Delta U_i = U_0 - U_i$
Rotor-based velocity deficit root sum square (RVDRSS) [17]	$U = U_0 - \sqrt{\sum_{i=1}^{n}(U_{h,i} - u_i)^2}$	$\Delta U_i = U_{h,i} - U_i$
Ambient-based energy deficit linear sum (AEDLS) [34]	$U = \sqrt{U_0^2 - \sum_{i=1}^{n}(U_0^2 - U_i^2)}$	$\Delta U_i = U_0 - U_i$
Rotor-based energy deficit linear sum (REDLS) [13]	$U = \sqrt{U_0^2 - \sum_{i=1}^{n}(U_{h,i}^2 - U_i^2)}$	$\Delta U_i = U_{h,i} - U_i$

3.2. Horn Rev 1 Wind Farm

The Horns Rev offshore wind farm is situated in the eastern North Sea in Denmark, and the first phase, consisting of 80 Vestas V-80 2 MW wind turbines (Horns Rev 1), was operated in 2002. The whole wind farm has a rhomboid distribution and the layout of wind turbines is illustrated in Figure 6. Basic parameters of the wind turbine, including the rotor diameter, the hub height, and the cut-in and cut-off velocities are provided by the manufacturer and shown in Table 6. The thrust coefficient C_T and power curves P are illustrated in Figure 7 and the specific values at a special inflow wind velocity are calculated by the linear interpolation method. The operational conditions are also shown in Table 6, i.e., the inflow velocity, the ambient turbulence intensity, and the aerodynamic surface roughness.

The wake models for multiple wind turbines are validated by numerical simulations carried out by Wu and Porte-Agel [35] where the turbine wake and power loss of the Horns Rev 1 offshore wind farm are numerically studied.

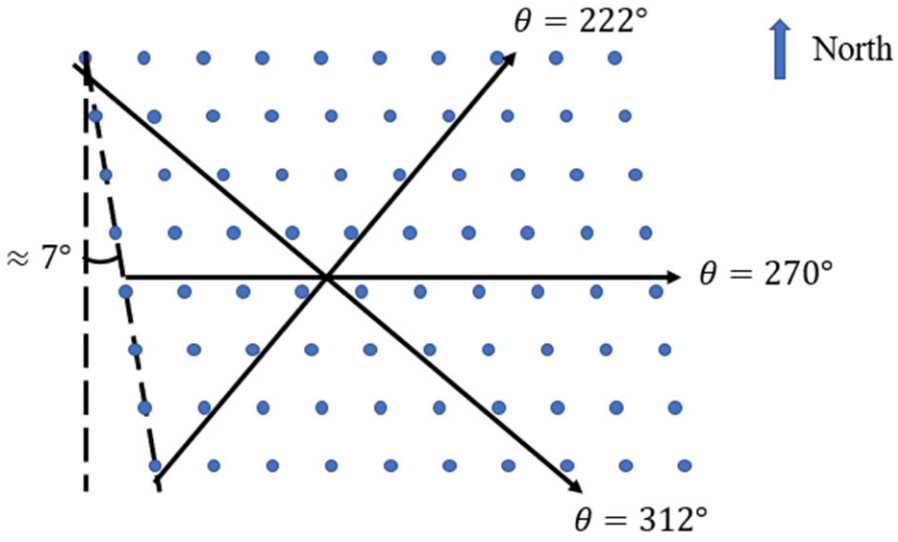

Figure 6. Wind turbine layout of the Horn Rev 1 wind farm.

Table 6. Basic parameters of the wind turbine and operational conditions of the wind farm.

	Basic Parameters	Values
The Vestas V-80 2 MW wind turbine	Rotor diameter	$D = 80\ m$
	Hub height	$z_{hub} = 70\ m$
	Cut-in wind velocity	$4\ m/s$
	Cut-off wind velocity	$25\ m/s$
The Horn Rev 1 wind farm	Inflow wind velocity	$8\ m/s$
	Ambient turbulence intensity	0.077
	Aerodynamic surface roughness	$0.0002\ m$
	Minimum turbine spacing	$7D$

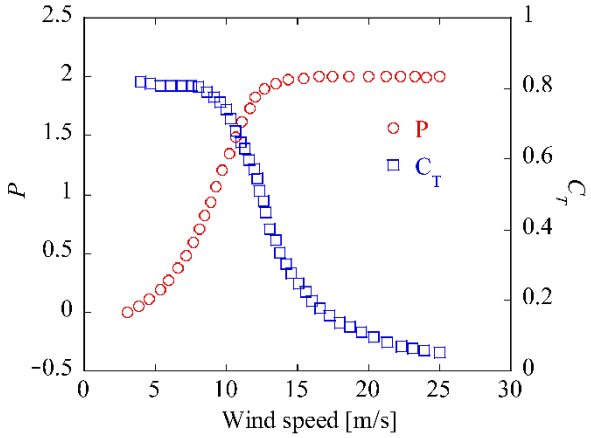

Figure 7. Thrust coefficient C_T and power curves P of the wind turbine [35].

4. Results and Discussions

The combined wake models for both single and multiple wind turbines are proposed and validated by numerical and experimental results in Section 4.1 and in Section 4.2, respectively. Effects of thrust coefficient and ambient turbulence intensity are studied in Section 4.3 and in Section 4.4, respectively.

4.1. Single Wind Turbine

To propose a wake model for predictions of velocity deficit, the spanwise distributions and wake boundary expansion models should be determined. The added turbulence intensity models and the superposition approaches for turbulence intensity should also be taken into account if the nonlinear wake boundary expansion model is used. In this study, modified wake models combined by different spanwise distributions mentioned in Section 2.1 with different wake boundary expansion models introduced in Section 2.2 are proposed to improve the accuracy and versatility. There are in total 70 combined wake models, and these are shown in the Appendix A in Table A1.

To validate the combined wake models, a series of numerical simulations, wind tunnel tests, and field tests were summarized from the previous studies and the basic parameters of measurements and simulations, including ambient turbulence intensity, thrust coefficient, aerodynamic surface roughness, hub height, rotor diameter, and normalized downstream distances are shown in Table 7. The aerodynamic surface roughness z_0 for simulations carried out by Ishihara and Qian is unknown, and they are defined as the same values with simulations by Wu and Porté-Agel [29] due to the similar ambient turbulence intensity.

Table 7. Descriptions of basic parameters of measurements and simulations.

Ref	I_0	C_T	z_0	z_h	D	x/D
	[-]	[-]	[m]	[m]	[m]	[-]
Wu and Porté-Agel [29]	0.134	0.8	0.5	70	80	5/7/10
	0.094	0.8	0.05	70	80	5/7/10
	0.069	0.8	0.005	70	80	5/7/10
	0.048	0.8	0.00005	70	80	5/7/10
Ishihara and Qian [5]	0.035	0.36	0.00005	80	76.5	6/8
	0.035	0.84	0.00005	80	76.5	6/8
	0.137	0.36	0.5	80	76.5	6/8
	0.137	0.84	0.5	80	76.5	6/8
Keane [11]	0.05	0.828	0.0002	91.5	116	5.03/5.3
Schreiber et al. [36]	0.05	0.75	0.0002	0.8	1.1	6/9
Gao et al. [33]	0.14	0.7	0.5	65	-	5/6
Zhang et al. [7]	0.13	0.62	0.075	50	43.2	5/7.5/10
	0.13	0.85	0.075	50	43.2	5/7.5
Tian et al. [6]	0.1	0.85	0.07	45	40	7.5
	0.1	0.75	0.07	45	40	5.5/8
Bastankhah and Porté-Agel [37]	0.067	0.78	0.000019	0.125	0.15	5/6/7/8

In general, to validate the wake model, a specific case with the known thrust coefficient and ambient turbulence intensity is considered, and the measurement and prediction data at a special downstream distance in the spanwise direction are compared. In this study, a comprehensive comparison is conducted to validate every combined wake model where all the measurements in Table 7 are used. To prevent the redundant comparisons between predictions and case-by-case measurements, we put all the prediction and measurement data in one figure and the hit rate q [38] is adopted as index to quantitatively evaluate the accuracy and versatility of combined wake models. It is expressed as follows:

$$q = \frac{1}{N_t}\sum_{i=1}^{N_t} n_i \quad with \quad n_i = \begin{cases} 1 & \left|\frac{p_i - m_i}{m_i}\right| \le D_q \ \ or \ \ |p_i - m_i| \le W_q \\ 0 & else \end{cases} \tag{10}$$

where m_i and p_i refer to measurements and predictions data for a special value i. N_t presents the total number of prediction data. The threshold values are followed by the German VDI guideline 3783-9 where $D_q = 0.25$ and $W_q = 0.07|max|$ [39].

The velocity deficit at the hub height in the spanwise direction at different downstream distances for every case in Table 7 is used to compute the hit rate. The combined wake models with the top 12 highest hit rates are listed in Table 8 and comparisons between predictions by combined wake models and measurements are illustrated in Figure 8. The blue lines show the threshold values followed by the German VDI guideline 3783-9 [39]. It is obvious that most points fall within the threshold range for the No. 3, No. 9, No. 29, and No. 13 combined wake models which means they have the higher hit rate. It was found that the No. 3 [7] and No. 9 wake models have the highest hit rate with q = 0.92, which means that the wake models are more universal than others. It was interesting to find that, compared with the IQ model (No. 15) by Ishihara and Qian [5], the No. 29 wake model combining the streamwise function by Bastankhah and Porté-Agel [4] with the linear wake boundary expansion model by Ishihara and Qian [5] had a higher hit rate.

Table 8. Combined wake models with top 12 hit rates.

No.	Spanwise Distribution	Streamwise Function	Wake Boundary Expansion	Added Turbulence Intensity	Turbulence Intensity	Hit Rate
3	Cosine	Zhang model	Non-linear (Z)	Crespo and Hernandez model	Square and root	0.92
9	Cosine	Zhang model	Non-linear (Z)	Larsen model	Square and root	0.92
29	Gaussian	BP model	Linear (IQ)	N/A	N/A	0.91
13	Cosine	Zhang model	Non-linear (Z)	IEC model	Linear sum	0.9
34	Gaussian	BP model	Non-linear (Z)	Frandsen model	Square and root	0.9
12	Cosine	Zhang model	Non-linear (Z)	IEC model	Square and root	0.89
35	Gaussian	BP model	Non-linear (Z)	Frandsen model	Linear sum	0.89
17	Gaussian	IQ model	Non-linear (Z)	Crespo and Hernandez model	Square and root	0.88
20	Gaussian	IQ model	Non-linear (Z)	Frandsen model	Square and root	0.88
21	Gaussian	IQ model	Non-linear (Z)	Frandsen model	Linear sum	0.88
23	Gaussian	IQ model	Non-linear (Z)	Larsen model	Square and root	0.88
28	Gaussian	IQ model	Non-linear (Z)	IEC model	Root and square	0.88

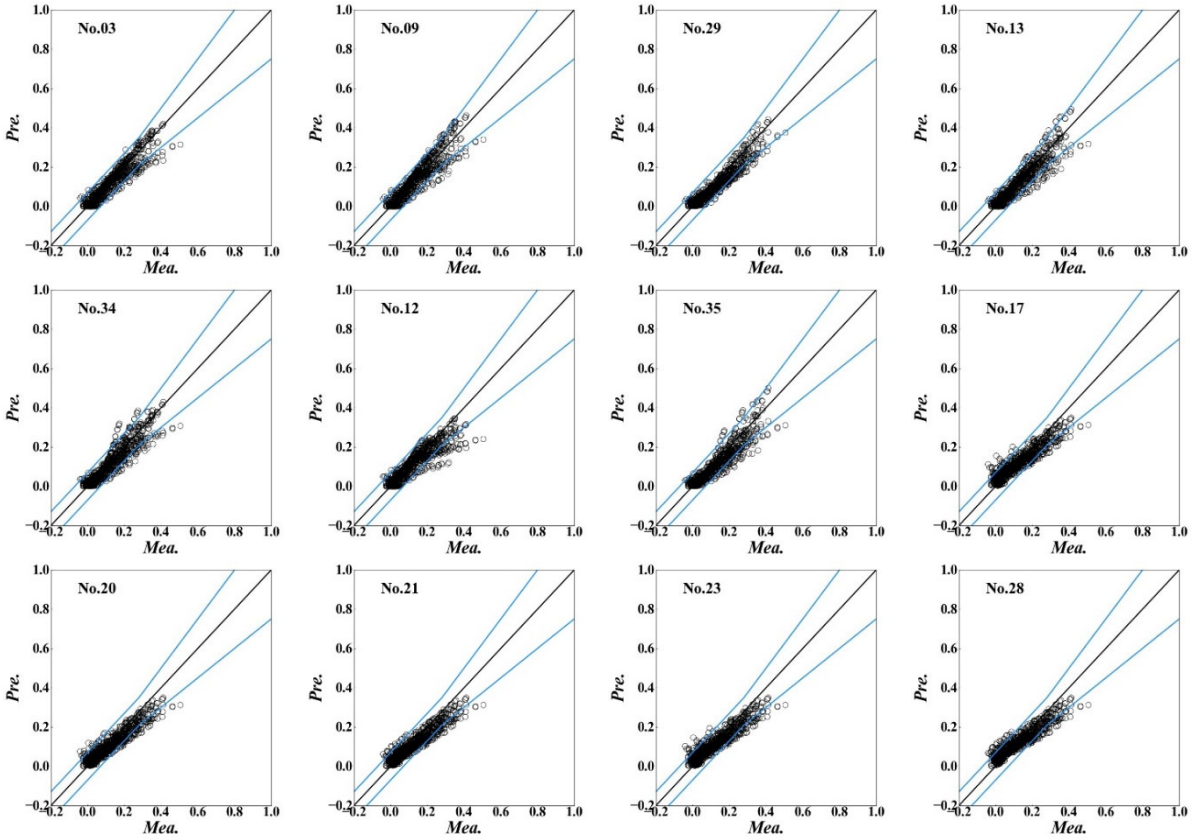

Figure 8. Comparison between predictions by combined wake models and measurements (blue line: threshold values; black line: *Mea.* = *Pre*; dot: velocity deficit).

4.2. Multi Wind Turbines

Wind farms generally consist of tens or hundreds of wind turbines to improve the efficiency of wind power generation. To accurately evaluate turbine wakes and power loss for multiple turbines, it is necessary to properly combine the single wake model and the superposition approach.

In this section, 70 combined wake models for the single wind turbine mentioned above will be checked whether they can be adopted to evaluate turbine wakes in wind farms and the proper superposition approach will also be chosen to combine with the single turbine wake model. Numerical simulations of turbine wakes in a row carried out by Wu and Porté-Agel [35] were used to validate the combination method. To save time and effort, the inflow wind velocity of the second wind turbine was firstly calculated by the single

turbine wake model and the process would be stopped if the inflow wind velocity was far different from the numerical results. On the contrary, the single turbine wake model accompanied with different superposition approaches was considered to calculate the wind velocity, turbulence intensity, and power generation of every wind turbine in a row. It was observed that predictions by the following five models for multiple wind turbines match well with simulations, while results predicted by other models are either underestimated or overestimated and they are not shown in this manuscript.

Figure 9 illustrates comparisons of velocity deficit, turbulence intensity, and power generation between simulation and prediction results by the No. 29 combined wake model with different superposition approaches. The wind speed and power generation are normalized by the inflow wind velocity and the wind power generation by the first wind turbine, respectively. It is noted that the rotor-based energy deficit linear superposition approach is more suitable for the No. 29 combined wake model and the predicted results show excellent agreement with simulations. However, the predicted results are either overestimated or underestimated by other superposition approaches. As for the turbulence intensity, the Crespo and Hernandez model is adopted and the added turbulence intensity induced by the closest upwind turbine is considered. As shown in Figure 10, the results by the No. 37 combined wake model with the rotor-based velocity deficit root sum square approach matches well with numerical simulations. In summary, both the No. 29 and the No. 37 combined wake models show their good performance for predictions of turbine-induced velocity deficit, turbulence intensity, and wind power generation in a wind farm.

It is also noted that predictions by the ambient-based energy deficit linear sum approach are the smallest, while results by the rotor-based velocity deficit root sum square approach are the largest in Figures 9–11. The rotor-based energy deficit linear sum and the rotor-based velocity deficit linear sum approaches are moderate. In fact, prediction errors by wake models always exist and these errors may be accumulated by the superposition approaches. Therefore, it is necessary to choose the wake model and the superposition approach properly. In this study, it is recommended that the No. 29 combined wake model and the rotor-based energy deficit linear sum approach.

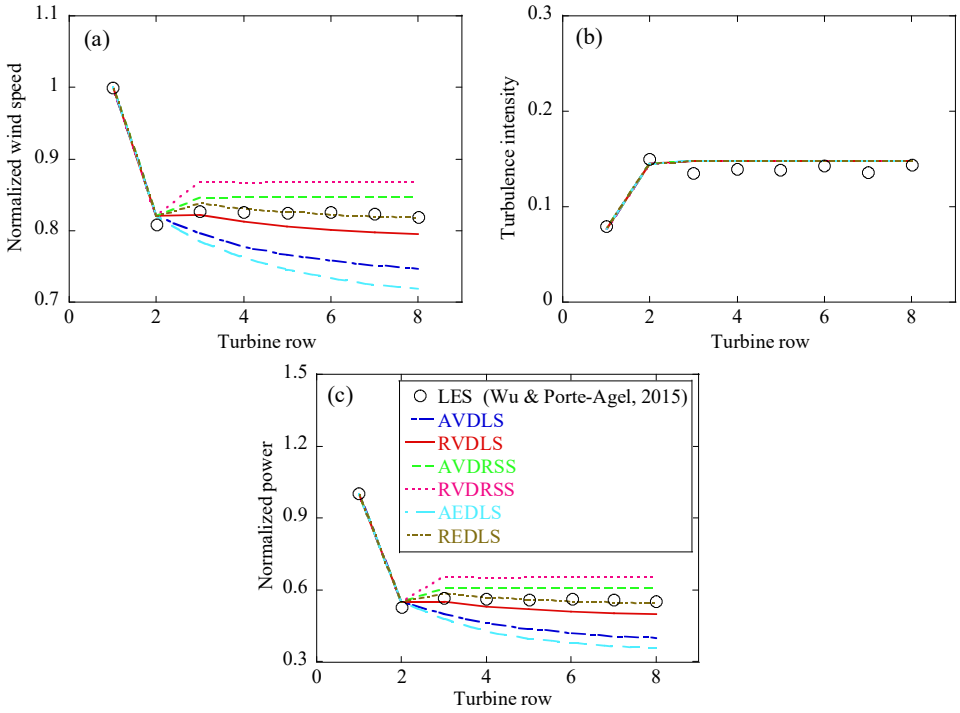

Figure 9. Comparisons of: (**a**) velocity deficit; (**b**) turbulence intensity; (**c**) power generations between simulations and predictions by the No. 29 combined wake model with different superposition approaches.

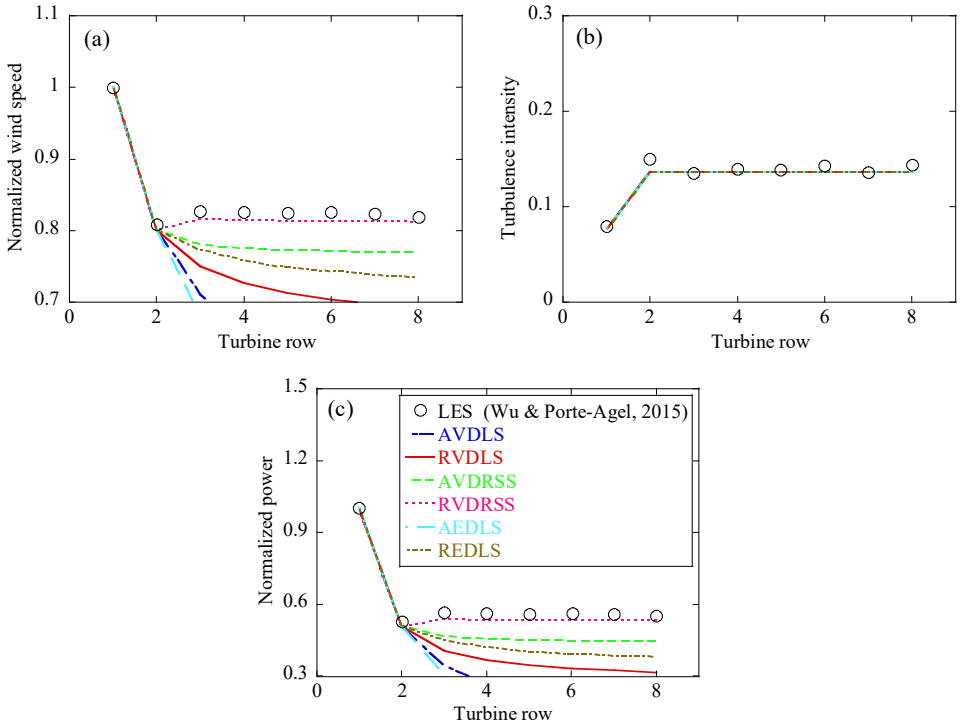

Figure 10. Comparisons of: (**a**) velocity deficit; (**b**) turbulence intensity; (**c**) power generations between simulations and predictions by the No. 37 combined wake model with different superposition approaches.

In addition, it is interesting to note that turbine-induced velocity deficit and wind power generation for multiple turbines in a row can be accurately predicted by the top-hat type wake models, including the No. 46, No. 47, No. 52, and No. 53 combined wake models while the turbulence intensities are underestimated as illustrated in Figure 11. The top-hat type wake models cannot accurately evaluate the velocity deficit for a single wind turbine since spanwise distributions are different from measured wake data and they maintain the same value over the whole rotor area. However, they neglect the process to calculate the equivalent velocity as shown in Equation (9) which may induce some errors.

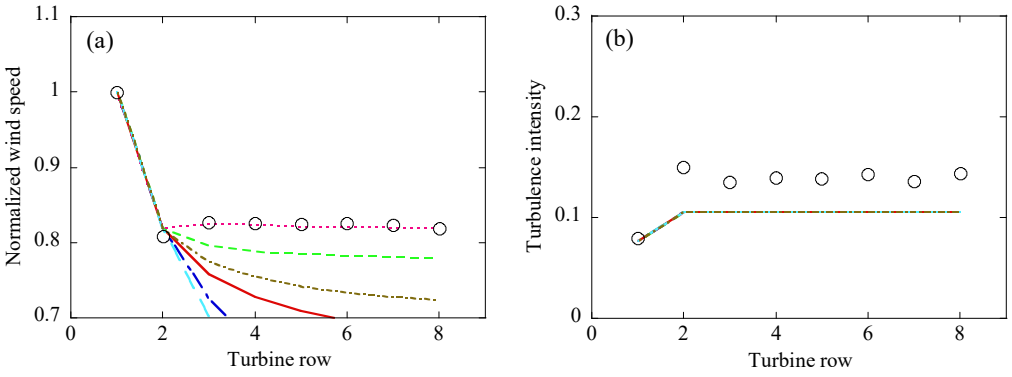

Figure 11. *Cont.*

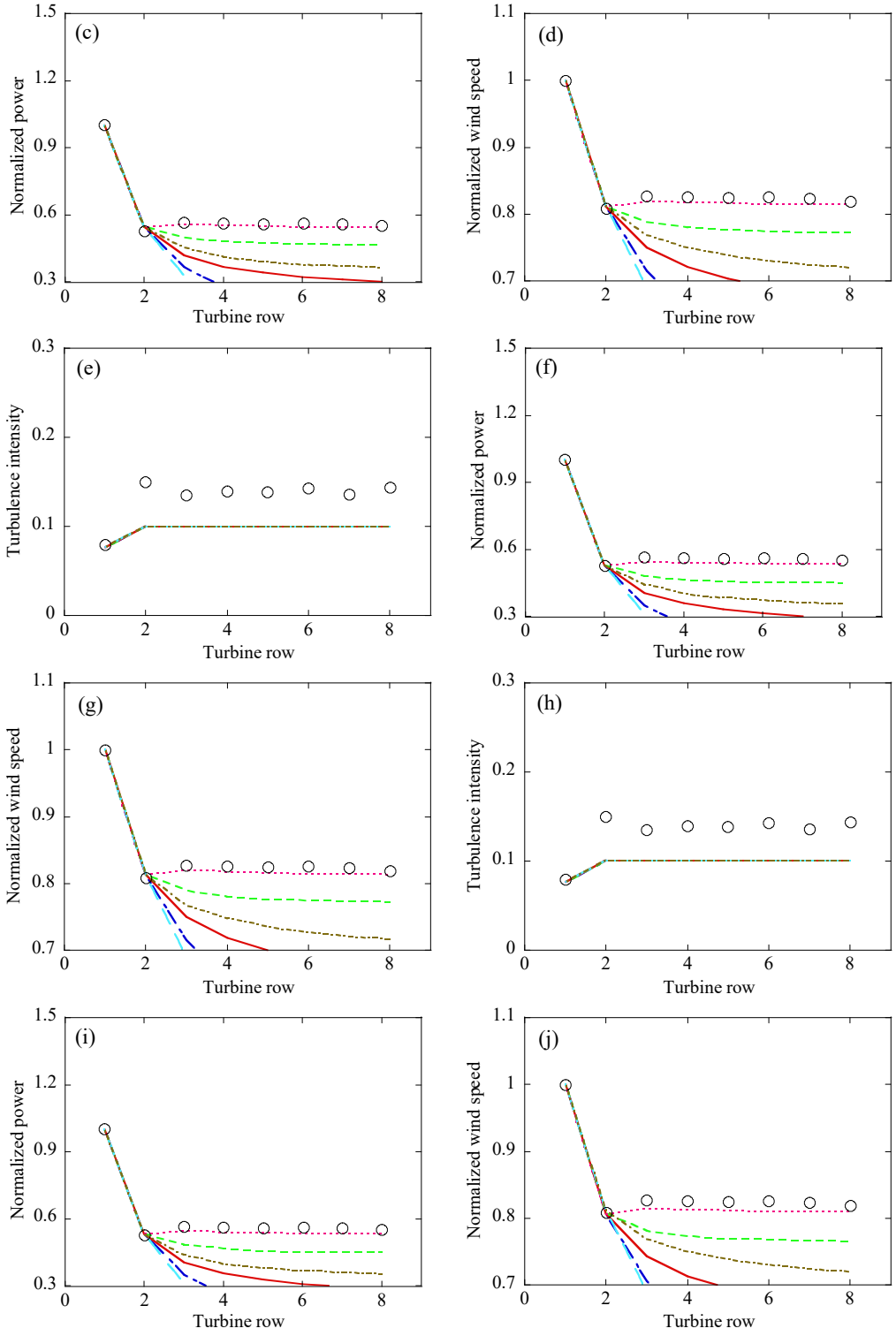

Figure 11. *Cont.*

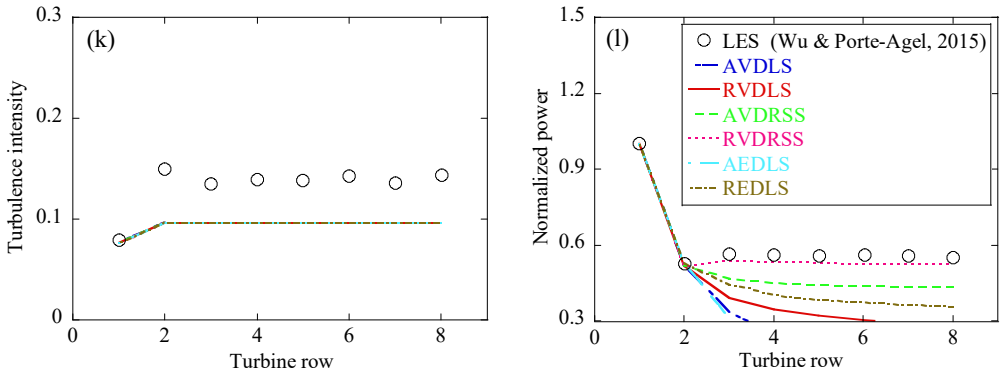

Figure 11. Comparisons of velocity deficit, turbulence intensity and power generations between simulations and predictions by: (**a**–**c**) the No. 46 combined wake model; (**d**–**f**) the No. 47 combined wake model; (**g**–**i**) the No. 52 combined wake model; (**j**–**l**) the No. 53 combined wake model; with different superposition approaches.

4.3. Effect of Thrust Coefficient

The thrust coefficient has an essential influence on the wake boundary expansion and velocity deficit. Simultaneously, it is determined by the inflow velocity at hub height as shown in Figure 7. In a wind farm, the inflow wind velocity cannot be a constant value, and it always changes in nature. Therefore, it is necessary to discuss the effect of thrust coefficient on the velocity, turbulence intensity, and power generation for multiple turbines in a row.

Three different thrust coefficients including $C_T = 0.8$, $C_T = 0.6$ and $C_T = 0.4$, are discussed in this study, and the corresponding inflow velocities at the hub height are $U_0 = 8\ m/s$, $U_0 = 11.6\ m/s$ and $U_0 = 13.1\ m/s$. The ambient turbulence intensity and aerodynamic surface roughness maintain the same values with the numerical simulations [35].

Figure 12 shows the velocity, turbulence intensity, and power generation of multiple wind turbines in a row by the No. 29 combined wind turbine and the rotor-based energy deficit linear sum approach under different thrust coefficients. It is obvious that the wind velocity and wind power generation will increase as the thrust coefficient decreases mainly because the inflow wind speed rises. The normalized wind velocity and power generation are normalized by the inflow wind speed and the power generation of the first wind turbine when the thrust coefficient is 0.8. They have the same variation trend along the downstream distance as the thrust coefficient changes. As for the turbulence intensity, it decreases as the thrust coefficient decreases. At this moment, the wind speed can pass through the turbine disk easily due to the reduction of thrust coefficient and turbulence generated by blades decreases accordingly. In fact, the thrust coefficient is not an independent parameter and it is determined by the inflow wind velocity at the hub height. Therefore, the effects of inflow wind velocity and thrust coefficient are studied together.

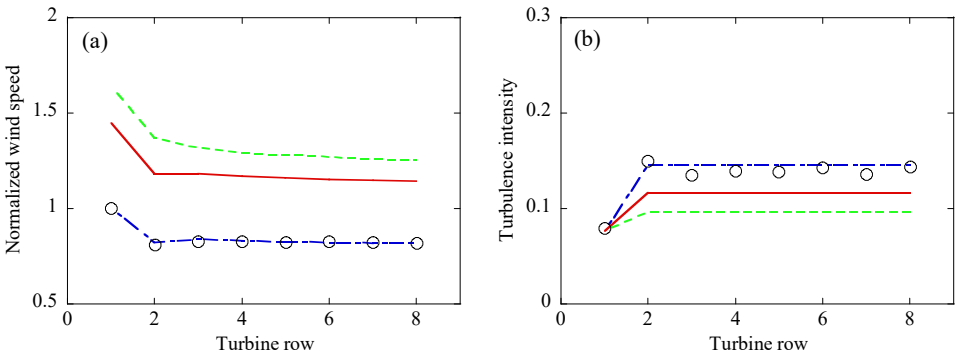

Figure 12. *Cont.*

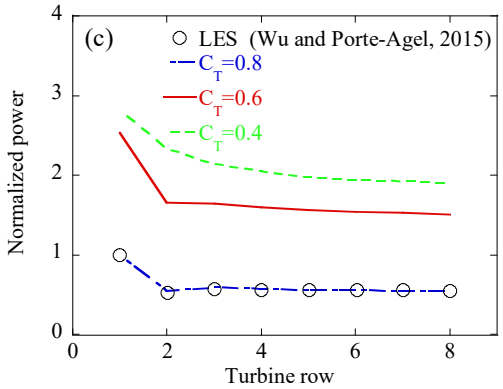

Figure 12. Effect of thrust coefficient on: (**a**) wind velocity; (**b**) turbulence intensity; (**c**) wind power generation of wind turbines in a row.

4.4. Effect of Ambient Turbulence Intensity

The ambient turbulence intensity affects the flow mixing in the wake region and the wake boundary expansion. For offshore wind farms, the wind speed is stable and the ambient turbulence intensity is generally low, but it will still vary slightly. Therefore, three ambient turbulence intensities, namely $I_0 = 0.05$, $I_0 = 0.06$, and $I_0 = 0.077$, are considered in this section. At this moment, other parameters will not be changed.

The effect of ambient turbulence intensity on velocity, turbulence intensity, and power generation of multiple wind turbines is studied as illustrated in Figure 13. The No. 29 combined wake model and the rotor-based energy deficit linear sum approach are used as well. It is observed that the ambient turbulence intensity has slight effects on the turbine-induced velocity deficit, turbulence intensity, and wind power generation in Figure 13 since its variation is limited. In fact, the downstream wind speed in front of the second wind turbine increases slightly as the ambient turbulence intensity rises due to the acceleration of flow mixing. The ambient turbulence intensity is an independent ambient parameter which will not be affected by the inflow wind velocity and the turbine condition. It is assumed that the ambient turbulence intensity maintains around 5% in the offshore wind farm. At this moment, the wind velocity and power generation will scarcely be affected by the ambient turbulence intensity.

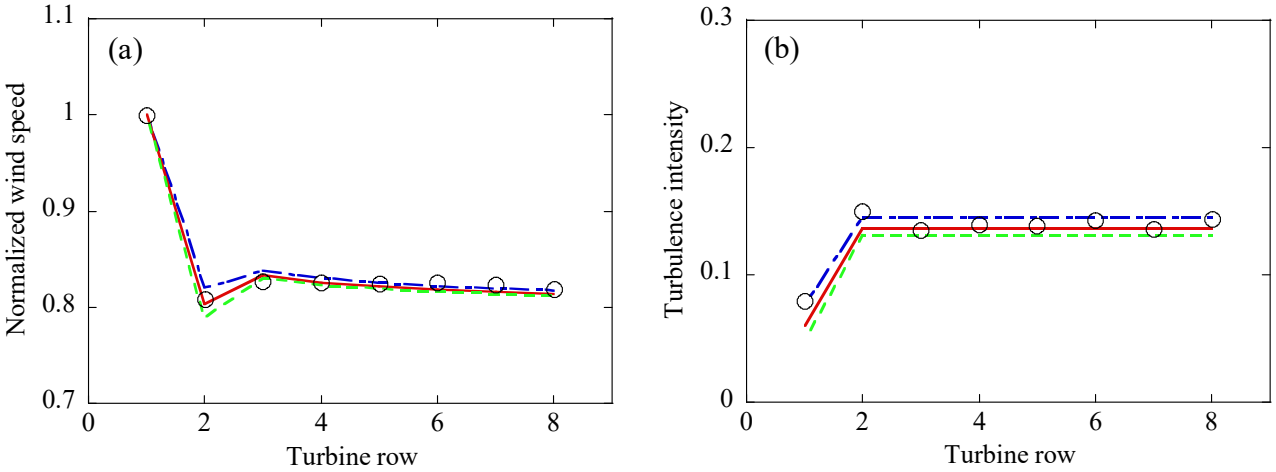

Figure 13. *Cont.*

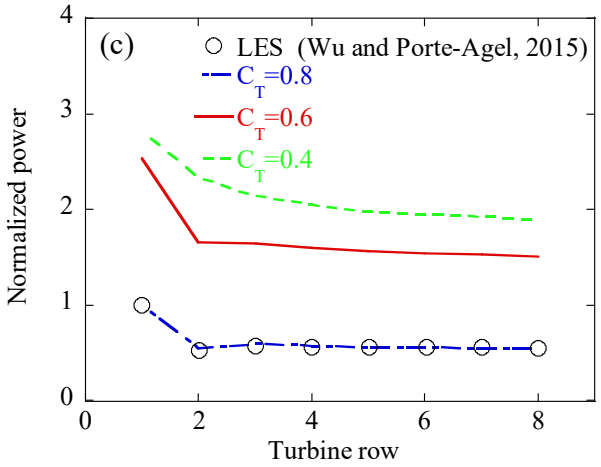

Figure 13. Effect of ambient turbulence intensity on: (**a**) wind velocity; (**b**) turbulence intensity; (**c**) wind power generation of wind turbines in a row.

5. Concluding Remarks

This paper investigated the applicability of wake models to predict turbine-induced velocity deficits and wind power generations for both single and multi-wind turbines. The conclusions are summarized as follows:

1. A series of wake models for a single wind rubine are proposed by combining different spanwise distributions and wake boundary expansion models. Compared with measurement data, the top 12 wake models ranked by the hit rate are summarized and they are more universal and accurate than others, especially for the No. 3, No. 9, and No. 29 combined wake models, which are considered as the most suitable wake models for the single wind turbine.
2. The wake models for multiple wind turbines are proposed by considering combined wake models for the single wind turbine and six superposition approaches. It is recommended that the No. 29 wake model combined with the rotor-based energy deficit linear superposition approach and the No. 37 wake model combined with the rotor-based velocity deficit root sum square approach should be used to carry out wind farm layout optimization due to their accurate predictions of velocity, turbulence intensity, and power generation for multiple wind turbines.
3. The effects of thrust coefficient and ambient turbulence intensity on the velocity, turbulence intensity, and wind power generation are investigated. It is found that the wind velocity as well as wind power generation increase, and the turbulence intensity decreases as the thrust coefficient reduces, whilst they almost maintain the same value as the ambient turbulence intensity varies.

Author Contributions: Conceptualization, G.H. and D.Z.; methodology, G.H. and D.Z.; software, D.Z. and Y.L.; validation, D.Z. and Y.L.; formal analysis, D.Z. and Y.L.; investigation, D.Z.; resources, G.H.; data curation, D.Z.; writing—original draft preparation, D.Z. and Y.L.; writing—review and editing, D.Z., G.H. and C.L.; visualization, D.Z. and Y.L.; supervision, G.H., C.L. and Y.X.; project administration, G.H.; funding acquisition, G.H. All authors have read and agreed to the published version of the manuscript.

Funding: This study is supported by National Key R&D Program of China (2021YFC3100702), National Natural Science Foundation of China (52108451), Shenzhen Science and Technology Innovation Commission (SGDX20210823103202018, GXWD20201230155427003-20200823230021001), Shenzhen Key Laboratory Launching Project (ZDSYS20200810113601005), and Guangdong-Hong Kong-Macao Joint Laboratory for Data-Driven Fluid Mechanics and Engineering Applications (2020B1212030001).

Conflicts of Interest: The authors declare no conflict of interest.

Nomenclature

a	axial flow induction factor
a_1	parameter in IQ model
A_0	cross-sectional area of rotor
A_W	cross-sectional area of downwind wake
b	parameter in IQ model
c	parameter in IQ model
C_T	thrust coefficient
$C(x)$	streamwise function of outside Gaussian flow for velocity deficit
D	rotor diameter
D_q	first threshold of hit rate
D_W	wake diameter downwind of the rotor
$G(r)$	spanwise functions of velocity deficit
I_+	added turbulence intensity
I_0	ambient turbulence intensity
I_w	wake turbulence intensity
k	wake expansion rate in the far wake region
K	constant in Frandsen model
K_n	empirical constant in Frandsen model
k_t	the constant rate of wake expansion
k_w	modified wake expansion rate in Zhang model
m_i	measured data
n	the total number of wind turbines
N_t	the total number of prediction data
P	wind power
P_i	predicted data
q	hit rate
r	radial distance from rotor center
r_0	rotor radius
$r_{1/2}$	half width of the wake
r_w	wake boundary at one special streamwise distance
U	wake velocity
$U_{h,i}$	the inflow velocity for ith wind turbine at hub height
U_i	the wake velocity of the ith wind turbine
U_0	inflow wind velocity
U_W	streamwise velocity downwind of the rotor
W_q	second threshold of hit rate
x	streamwise distance downstream wind turbine
y	spanwise distance downstream wind turbine
z_0	surface roughness length
z_h	the turbine hub height

Greek Symbols

α	empirical constant in Frandsen model
β	wake expansion parameter in Frandsen model
ε	intercept in IQ model
ΔI	streamwise function of the added turbulence intensity
ΔU_i	wake velocity deficit of the ith wind turbine
ΔU	wake velocity deficit
ΔU_{max}	wake velocity deficit at hub height
θ	wind angle
ρ	air density
σ	standard deviation of Gaussian wake velocity deficit

Appendix A

All the combined wake models are shown in Table A1 considering different spanwise distributions, streamwise functions, wake boundary expansion models, added turbulence intensity models, and the superposition approaches for turbulence intensity. The hit rate q for every combined wake model is calculated by comparing prediction and measurement data. To provide a comprehensive comparison, the wake models proposed by previous studies have also been added in Table A1, such as the No. 3 [7], No. 15 [5], No. 34 [13], and No. 58 [3] wake models. The comparisons of the combined wake models are shown in Figures A1–A5. For the single wind turbine, it is obviously noted that combined wake models with Gaussian and cosine-shaped distributions have high hit rates, which mean they can be used to accurately predict the turbine-induced velocity deficit while the models with the top-hat distribution have low hit rates since the spanwise distributions are different from measurement data.

Table A1. Descriptions of the combined wake models.

Case	Spanwise Distribution	Streamwise Function	Wake Boundary Expansion	Added Turbulence Intensity	Turbulence Intensity	Hit Rate
1	Cosine	Zhang model	Linear (IQ)	-	-	0.55
2	Cosine	Zhang model	Non-linear (F)	-	-	0.48
3	Cosine	Zhang model	Non-linear (Z)	Crespo and Hernandez model	Square and root	0.92
4	Cosine	Zhang model	Non-linear (Z)	Crespo and Hernandez model	Linear sum	0.68
5	Cosine	Zhang model	Non-linear (Z)	Crespo and Hernandez model	Root and square	0.64
6	Cosine	Zhang model	Non-linear (Z)	Frandsen model	Square and root	0.82
7	Cosine	Zhang model	Non-linear (Z)	Frandsen model	Linear sum	0.87
8	Cosine	Zhang model	Non-linear (Z)	Frandsen model	Root and square	0.87
9	Cosine	Zhang model	Non-linear (Z)	Larsen model	Square and root	0.92
10	Cosine	Zhang model	Non-linear (Z)	Larsen model	Linear sum	0.64
11	Cosine	Zhang model	Non-linear (Z)	Larsen model	Root and square	0.61
12	Cosine	Zhang model	Non-linear (Z)	IEC model	Square and root	0.89
13	Cosine	Zhang model	Non-linear (Z)	IEC model	Linear sum	0.9
14	Cosine	Zhang model	Non-linear (Z)	IEC model	Root and square	0.87
15	Gaussian	IQ model	Linear (IQ)	-	-	0.85
16	Gaussian	IQ model	Non-linear (F)	-	-	0.85
17	Gaussian	IQ model	Non-linear (Z)	Crespo and Hernandez model	Square and root	0.88
18	Gaussian	IQ model	Non-linear (Z)	Crespo and Hernandez model	Linear sum	0.87
19	Gaussian	IQ model	Non-linear (Z)	Crespo and Hernandez model	Root and square	0.86
20	Gaussian	IQ model	Non-linear (Z)	Frandsen model	Square and root	0.88
21	Gaussian	IQ model	Non-linear (Z)	Frandsen model	Linear sum	0.88
22	Gaussian	IQ model	Non-linear (Z)	Frandsen model	Root and square	0.87
23	Gaussian	IQ model	Non-linear (Z)	Larsen model	Square and root	0.88
24	Gaussian	IQ model	Non-linear (Z)	Larsen model	Linear sum	0.87
25	Gaussian	IQ model	Non-linear (Z)	Larsen model	Root and square	0.86
26	Gaussian	IQ model	Non-linear (Z)	IEC model	Square and root	0.86
27	Gaussian	IQ model	Non-linear (Z)	IEC model	Linear sum	0.87
28	Gaussian	IQ model	Non-linear (Z)	IEC model	Root and square	0.88
29	Gaussian	BP model	Linear (IQ)	-	-	0.91
30	Gaussian	BP model	Non-linear (F)	-	-	0.87
31	Gaussian	BP model	Non-linear (Z)	Crespo and Hernandez model	Square and root	0.84
32	Gaussian	BP model	Non-linear (Z)	Crespo and Hernandez model	Linear sum	0.84
33	Gaussian	BP model	Non-linear (Z)	Crespo and Hernandez model	Root and square	0.76
34	Gaussian	BP model	Non-linear (Z)	Frandsen model	Square and root	0.9
35	Gaussian	BP model	Non-linear (Z)	Frandsen model	Linear sum	0.89
36	Gaussian	BP model	Non-linear (Z)	Frandsen model	Root and square	0.76
37	Gaussian	BP model	Non-linear (Z)	Larsen model	Square and root	0.85
38	Gaussian	BP model	Non-linear (Z)	Larsen model	Linear sum	0.81
39	Gaussian	BP model	Non-linear (Z)	Larsen model	Root and square	0.75
40	Gaussian	BP model	Non-linear (Z)	IEC model	Square and root	0.76
41	Gaussian	BP model	Non-linear (Z)	IEC model	Linear sum	0.82
42	Gaussian	BP model	Non-linear (Z)	IEC model	Root and square	0.79
43	Top-hat	Jensen model	Linear (IQ)	-	-	0.47
44	Top-hat	Jensen model	Non-linear (F)	-	-	0.45
45	Top-hat	Jensen model	Non-linear (Z)	Crespo and Hernandez model	Square and root	0.46
46	Top-hat	Jensen model	Non-linear (Z)	Crespo and Hernandez model	Linear sum	0.48
47	Top-hat	Jensen model	Non-linear (Z)	Crespo and Hernandez model	Root and square	0.47
48	Top-hat	Jensen model	Non-linear (Z)	Frandsen model	Square and root	0.48

Table A1. *Cont.*

Case	Spanwise Distribution	Streamwise Function	Wake Boundary Expansion	Added Turbulence Intensity	Turbulence Intensity	Hit Rate
49	Top-hat	Jensen model	Non-linear (Z)	Frandsen model	Linear sum	0.48
50	Top-hat	Jensen model	Non-linear (Z)	Frandsen model	Root and square	0.46
51	Top-hat	Jensen model	Non-linear (Z)	Larsen model	Square and root	0.47
52	Top-hat	Jensen model	Non-linear (Z)	Larsen model	Linear sum	0.47
53	Top-hat	Jensen model	Non-linear (Z)	Larsen model	Root and square	0.47
54	Top-hat	Jensen model	Non-linear (Z)	IEC model	Square and root	0.47
55	Top-hat	Jensen model	Non-linear (Z)	IEC model	Linear sum	0.47
56	Top-hat	Jensen model	Non-linear (Z)	IEC model	Root and square	0.45
57	Top-hat	Frandsen model	Linear (IQ)	-	-	0.45
58	Top-hat	Frandsen model	Non-linear (F)	-	-	0.48
59	Top-hat	Frandsen model	Non-linear (Z)	Crespo and Hernandez model	Square and root	0.46
60	Top-hat	Frandsen model	Non-linear (Z)	Crespo and Hernandez model	Linear sum	0.46
61	Top-hat	Frandsen model	Non-linear (Z)	Crespo and Hernandez model	Root and square	0.47
62	Top-hat	Frandsen model	Non-linear (Z)	Frandsen model	Square and root	0.48
63	Top-hat	Frandsen model	Non-linear (Z)	Frandsen model	Linear sum	0.47
64	Top-hat	Frandsen model	Non-linear (Z)	Frandsen model	Root and square	0.46
65	Top-hat	Frandsen model	Non-linear (Z)	Larsen model	Square and root	0.46
66	Top-hat	Frandsen model	Non-linear (Z)	Larsen model	Linear sum	0.47
67	Top-hat	Frandsen model	Non-linear (Z)	Larsen model	Root and square	0.47
68	Top-hat	Frandsen model	Non-linear (Z)	IEC model	Square and root	0.48
69	Top-hat	Frandsen model	Non-linear (Z)	IEC model	Linear sum	0.46
70	Top-hat	Frandsen model	Non-linear (Z)	IEC model	Root and square	0.44

Linear (IQ), Non-linear (F) and Non-linear (Z): the linear or nonlinear wake boundary expansion models proposed by Ishihara and Qian [5]; by Frandsen et al. [3]; by Zhang et al. [7].

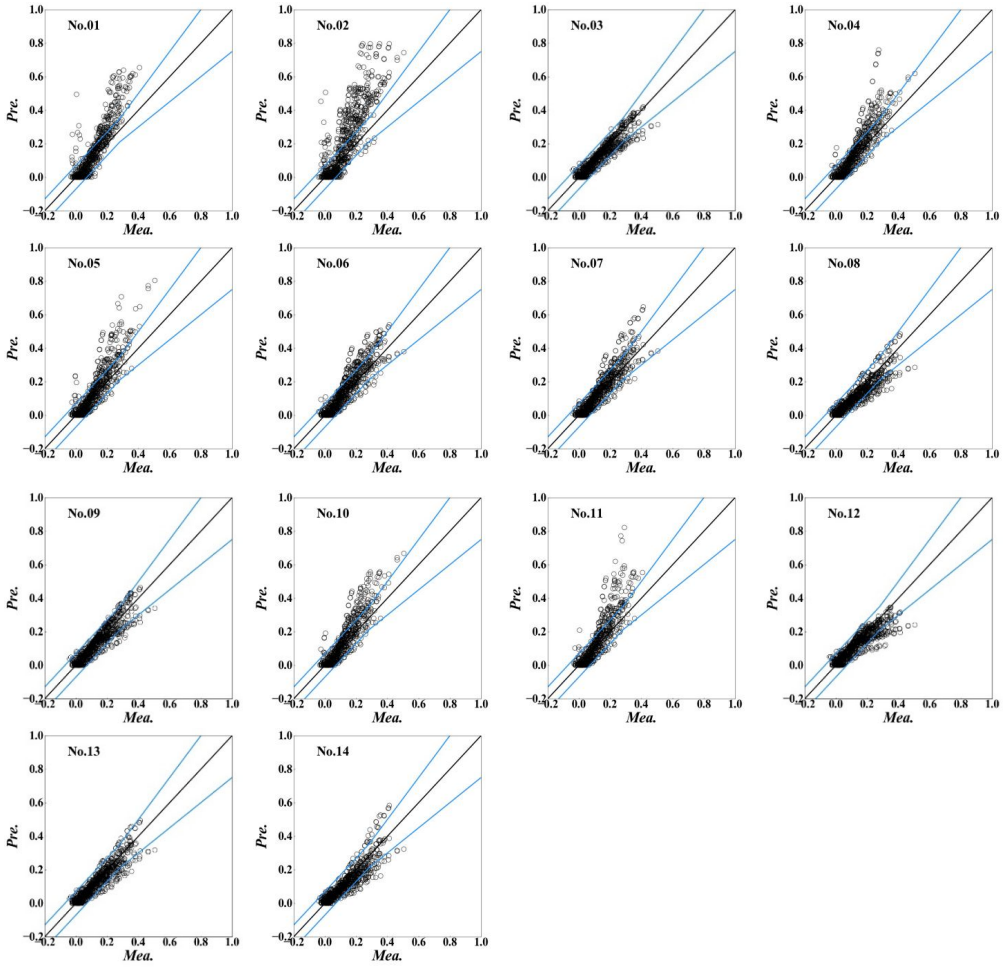

Figure A1. Comparisons of the combined wake models with the cosine-shaped distribution.

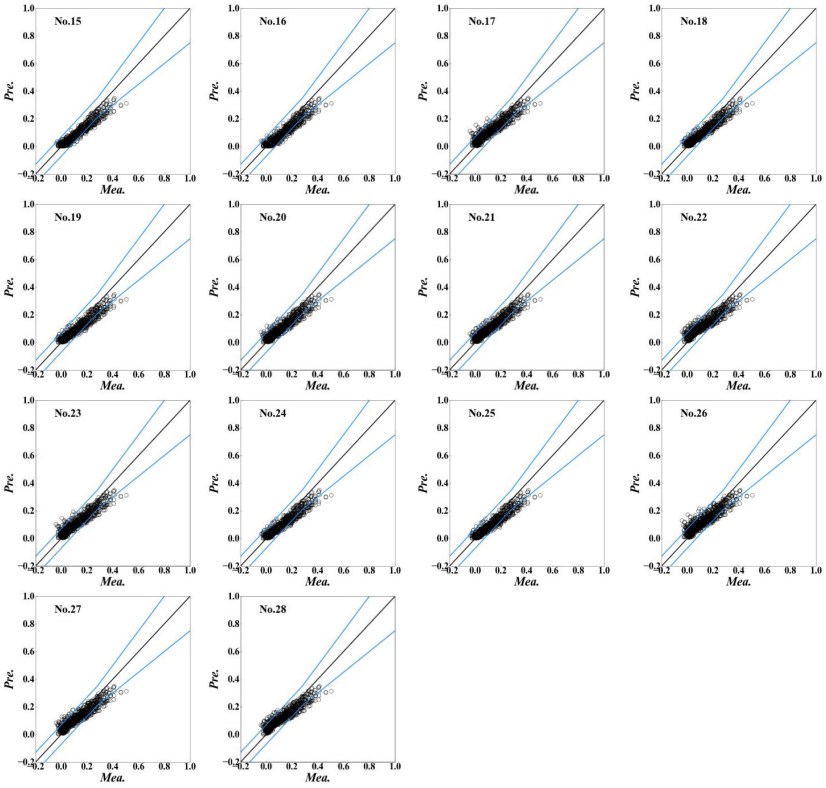

Figure A2. Comparisons of the combined wake models with the Gaussian distribution and the streamwise distribution of IQ model.

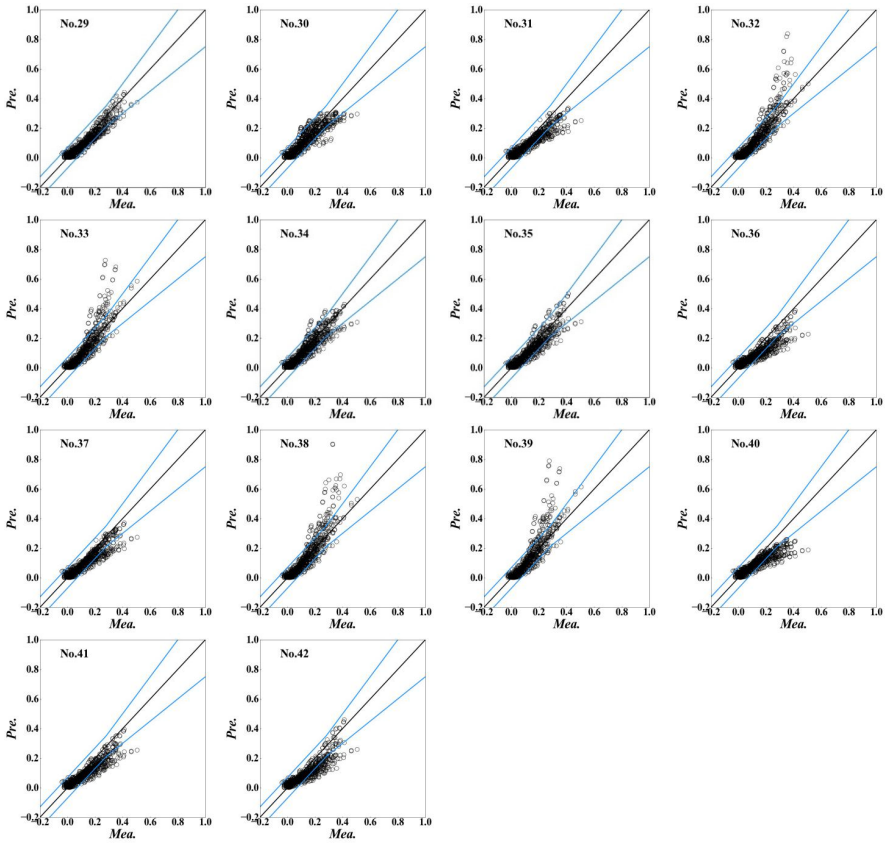

Figure A3. Comparisons of the combined wake models with the Gaussian distribution and the streamwise distribution of BP model.

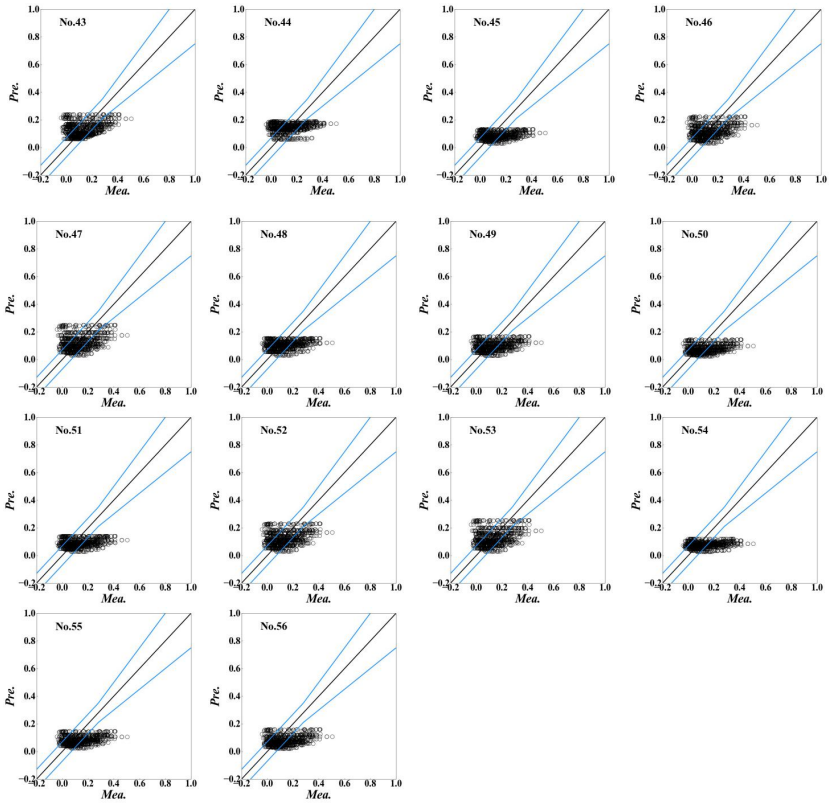

Figure A4. Comparisons of the combined wake models with the top-hat distribution and the streamwise distribution of Jensen model.

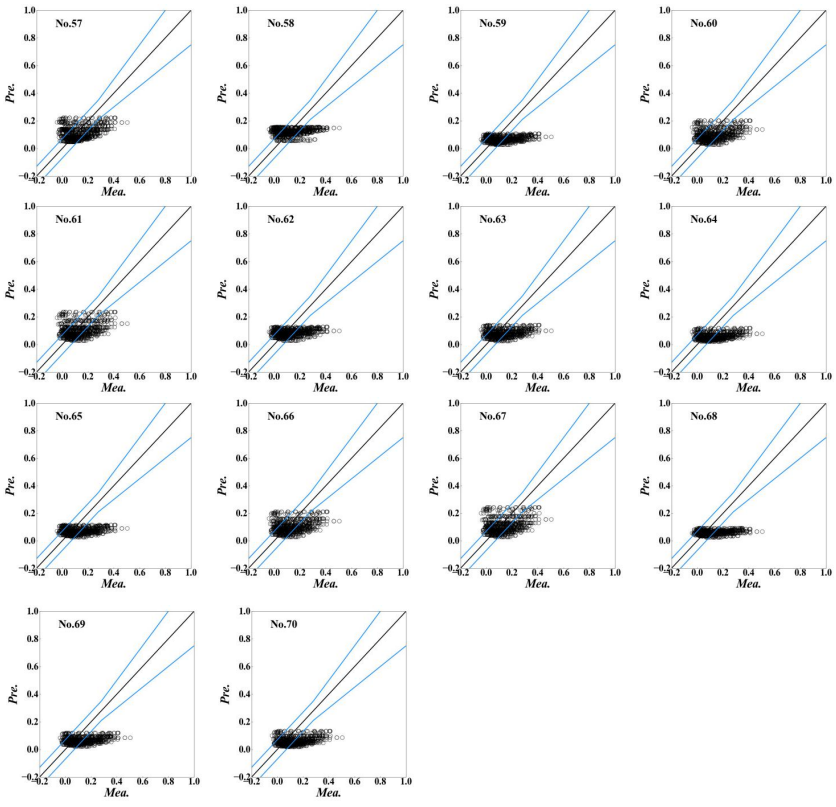

Figure A5. Comparisons of the combined wake models with the top-hat distribution and the streamwise distribution of Frandsen model.

References

1. GWEC. *Global Wind Report 2021*; Global Wind Energy Council: Brussels, Belgium, 2021.
2. Jensen, N.O. *A Note on Wind Generator Interaction*; Risø National Laboratory: Roskilde, Denmark, 1983.
3. Frandsen, S.; Barthelmie, R.; Pryor, S.; Rathmann, O.; Larsen, S.; Højstrup, J.; Thøgersen, M. Analytical Modelling of Wind Speed Deficit in Large Offshore Wind Farms. *Wind Energ.* **2006**, *9*, 39–53. [CrossRef]
4. Bastankhah, M.; Porté-Agel, F. A New Analytical Model for Wind-Turbine Wakes. *Renew. Energy* **2014**, *70*, 116–123. [CrossRef]
5. Ishihara, T.; Qian, G.-W. A New Gaussian-Based Analytical Wake Model for Wind Turbines Considering Ambient Turbulence Intensities and Thrust Coefficient Effects. *J. Wind Eng. Ind. Aerodyn.* **2018**, *177*, 275–292. [CrossRef]
6. Tian, L.; Zhu, W.; Shen, W.; Zhao, N.; Shen, Z. Development and Validation of a New Two-Dimensional Wake Model for Wind Turbine Wakes. *J. Wind Eng. Ind. Aerodyn.* **2015**, *137*, 90–99. [CrossRef]
7. Zhang, Z.; Huang, P.; Sun, H. A Novel Analytical Wake Model with a Cosine-Shaped Velocity Deficit. *Energies* **2020**, *13*, 3353. [CrossRef]
8. Gao, X.; Li, B.; Wang, T.; Sun, H.; Yang, H.; Li, Y.; Wang, Y.; Zhao, F. Investigation and Validation of 3D Wake Model for Horizontal-Axis Wind Turbines Based on Filed Measurements. *Appl. Energy* **2020**, *260*, 114272. [CrossRef]
9. Sun, H.; Yang, H. Study on an Innovative Three-Dimensional Wind Turbine Wake Model. *Appl. Energy* **2018**, *226*, 483–493. [CrossRef]
10. Ge, M.; Wu, Y.; Liu, Y.; Yang, X.I.A. A Two-Dimensional Jensen Model with a Gaussian-Shaped Velocity Deficit. *Renew. Energy* **2019**, *141*, 46–56. [CrossRef]
11. Keane, A. Advancement of an Analytical Double-Gaussian Full Wind Turbine Wake Model. *Renew. Energy* **2021**, *171*, 687–708. [CrossRef]
12. Wang, Y.; Lin, J.; Zhang, J. Investigation of a New Analytical Wake Prediction Method for Offshore Floating Wind Turbines Considering an Accurate Incoming Wind Flow. *Renew. Energy* **2022**, *185*, 827–849. [CrossRef]
13. Yang, Q.; Li, H.; Li, T.; Zhou, X. Wind Farm Layout Optimization for Levelized Cost of Energy Minimization with Combined Analytical Wake Model and Hybrid Optimization Strategy. *Energy Convers. Manag.* **2021**, *248*, 114778. [CrossRef]
14. Pillai, A.C.; Chick, J.; Khorasanchi, M.; Barbouchi, S.; Johanning, L. Application of an Offshore Wind Farm Layout Optimization Methodology at Middelgrunden Wind Farm. *Ocean Eng.* **2017**, *139*, 287–297. [CrossRef]
15. Kirchner-Bossi, N.; Porté-Agel, F. Realistic Wind Farm Layout Optimization through Genetic Algorithms Using a Gaussian Wake Model. *Energies* **2018**, *11*, 3268. [CrossRef]
16. Qian, G.-W.; Ishihara, T. Wind Farm Power Maximization through Wake Steering with a New Multiple Wake Model for Prediction of Turbulence Intensity. *Energy* **2021**, *220*, 119680. [CrossRef]
17. Lissaman, P.B.S. Energy Effectiveness of Arbitrary Arrays of Wind Turbines. *J. Energy* **1979**, *3*, 323–328. [CrossRef]
18. Niayifar, A.; Porté-Agel, F. Analytical Modeling of Wind Farms: A New Approach for Power Prediction. *Energies* **2016**, *9*, 741. [CrossRef]
19. Katic, I.; Højstrup, J.; Jensen, N.O. A Simple Model for Cluster Efficiency. In *EWEC'86. Proceedings*; European Wind Energy Association: Rome, Italy, 1987; pp. 407–410.
20. Voutsinas, S. On the Analysis of Wake Effects in Wind Parks. *Wind Eng.* **1990**, *14*, 204–219.
21. Göçmen, T.; van der Laan, P.; Réthoré, P.-E.; Diaz, A.P.; Larsen, G.C.; Ott, S. Wind Turbine Wake Models Developed at the Technical University of Denmark: A Review. *Renew. Sustain. Energy Rev.* **2016**, *60*, 752–769. [CrossRef]
22. Shao, Z.; Wu, Y.; Li, L.; Han, S.; Liu, Y. Multiple Wind Turbine Wakes Modeling Considering the Faster Wake Recovery in Overlapped Wakes. *Energies* **2019**, *12*, 680. [CrossRef]
23. Tian, L.; Zhu, W.; Shen, W.; Song, Y.; Zhao, N. Prediction of Multi-Wake Problems Using an Improved Jensen Wake Model. *Renew. Energy* **2017**, *102*, 457–469. [CrossRef]
24. Barthelmie, R.J.; Larsen, G.C.; Frandsen, S.T.; Folkerts, L.; Rados, K.; Pryor, S.C.; Lange, B.; Schepers, G. Comparison of Wake Model Simulations with Offshore Wind Turbine Wake Profiles Measured by Sodar. *J. Atmos. Ocean. Technol.* **2006**, *23*, 888–901. [CrossRef]
25. Barthelmie, R.J.; Jensen, L.E. Evaluation of Wind Farm Efficiency and Wind Turbine Wakes at the Nysted Offshore Wind Farm. *Wind Energy* **2010**, *13*, 573–586. [CrossRef]
26. Cleve, J.; Greiner, M.; Enevoldsen, P.; Birkemose, B.; Jensen, L. Model-Based Analysis of Wake-Flow Data in the Nysted Offshore Wind Farm. *Wind Energy* **2009**, *12*, 125–135. [CrossRef]
27. Barthelmie, R.J.; Frandsen, S.T.; Nielsen, M.N.; Pryor, S.C.; Rethore, P.-E.; Jørgensen, H.E. Modelling and Measurements of Power Losses and Turbulence Intensity in Wind Turbine Wakes at Middelgrunden Offshore Wind Farm. *Wind Energy* **2007**, *10*, 517–528. [CrossRef]
28. Ge, M.; Wu, Y.; Liu, Y.; Li, Q. A Two-Dimensional Model Based on the Expansion of Physical Wake Boundary for Wind-Turbine Wakes. *Appl. Energy* **2019**, *233–234*, 975–984. [CrossRef]
29. Wu, Y.-T.; Porté-Agel, F. Atmospheric Turbulence Effects on Wind-Turbine Wakes: An LES Study. *Energies* **2012**, *5*, 5340–5362. [CrossRef]
30. Crespo, A.; Hernández, J. Turbulence Characteristics in Wind-Turbine Wakes. *J. Wind Eng. Ind. Aerodyn.* **1996**, *61*, 71–85. [CrossRef]

31. Larsen, G.C.; Højstrup, J.; Madsen, H.A. Wind Fields in Wakes. In Proceedings of the 1996 European Wind Energy Conference and Exhibition, Göteborg, Sweden, 20–24 May 1996.
32. *IEC 61400-1*; Wind Turbine Generator Systems Part 1: Safety Requirements. International Electrotechnical Commission: Geneva, Switzerland, 2019.
33. Gao, X.; Yang, H.; Lu, L. Optimization of Wind Turbine Layout Position in a Wind Farm Using a Newly-Developed Two-Dimensional Wake Model. *Appl. Energy* **2016**, *174*, 192–200. [CrossRef]
34. Renkema, D.J. Validation of Wind Turbine Wake Models. Master's Thesis, TU Delft, Delft, The Netherlands, 2007.
35. Wu, Y.-T.; Porté-Agel, F. Modeling Turbine Wakes and Power Losses within a Wind Farm Using LES: An Application to the Horns Rev Offshore Wind Farm. *Renew. Energy* **2015**, *75*, 945–955. [CrossRef]
36. Schreiber, J.; Balbaa, A.; Bottasso, C.L. Brief Communication: A Double-Gaussian Wake Model. *Wind Energ. Sci.* **2020**, *5*, 237–244. [CrossRef]
37. Bastankhah, M.; Porté-Agel, F. A New Miniature Wind Turbine for Wind Tunnel Experiments. Part II: Wake Structure and Flow Dynamics. *Energies* **2017**, *10*, 923. [CrossRef]
38. Oettl, D. Quality Assurance of the Prognostic, Microscale Wind-Field Model GRAL 14.8 Using Wind-Tunnel Data Provided by the German VDI Guideline 3783-9. *J. Wind Eng. Ind. Aerodyn.* **2015**, *142*, 104–110. [CrossRef]
39. VDI. *Environmental Meteorology—Prognostic Microscale Windfield Models—Evaluation for Flow around Buildings and Obstacles*; Tech. Rep., VDI guideline 3783, Part 9; Beuth Verlag: Berlin, Germany, 2005.